Determination of the Collins-Soper Kernel from Lattice QCD

Artur Avkhadiev,[1] Phiala E. Shanahan,[1] Michael L. Wagman,[2] and Yong Zhao[3]
[1]*Center for Theoretical Physics, Massachusetts Institute of Technology, Cambridge, Massachusetts 02139, USA*
[2]*Fermi National Accelerator Laboratory, Batavia, Illinois 60510, USA*
[3]*Physics Division, Argonne National Laboratory, Lemont, Illinois 60439, USA*

(Received 11 March 2024; accepted 23 April 2024; published 3 June 2024)

This Letter presents a determination of the quark Collins-Soper kernel, which relates transverse-momentum-dependent parton distributions (TMDs) at different rapidity scales, using lattice quantum chromodynamics (QCD). This is the first such determination with systematic control of quark mass, operator mixing, and discretization effects. Next-to-next-to-leading logarithmic matching is used to match lattice-calculable distributions to the corresponding TMDs. The continuum-extrapolated lattice QCD results are consistent with several recent phenomenological parametrizations of the Collins-Soper kernel and are precise enough to disfavor other parametrizations.

DOI: 10.1103/PhysRevLett.132.231901

Elucidating the three-dimensional structure of the proton is a key target of current and future experimental programs worldwide, including the COMPASS [1–7] experiment at CERN, RHIC [8,9] at Brookhaven National Laboratory, the 12 GeV program [10–15] at Thomas Jefferson National Accelerator Facility, and future experiments at the planned Electron-Ion Collider [16–21]. In recent years, considerable developments have been made to constrain the proton's transverse structure, in particular, as parametrized by transverse-momentum-dependent parton distributions (TMDs) [22–24].

In this context, a quantity of particular importance is the Collins-Soper (CS) kernel: a fundamental nonperturbative function that appears as the universal rapidity evolution kernel for TMDs, which can be considered to characterize the QCD vacuum [22–24]. The CS kernel is not only a fundamental proton and nuclear structure observable of importance in its own right, it is also needed to compare TMDs measured at different scales and is required as input into measurements of electroweak observables including the W-boson mass [25] and in various nuclear structure studies [20].

Phenomenological extractions of the CS kernel from global fits of experimental data from Drell-Yan and semi-inclusive deep-inelastic scattering processes, however, are largely unconstrained in the nonperturbative region, with inconsistencies between different extractions arising, in particular, for kinematics with small transverse-momentum scale $q_T \lesssim 0.3$ GeV. First constraints of the CS kernel from lattice QCD calculations [26–35] demonstrate the potential of this approach to provide first-principles information with sufficient precision to distinguish between different phenomenological models in this regime. Nevertheless, key systematic uncertainties, in particular, discretization effects, remain to be controlled in all such calculations to date.

This Letter presents a new lattice QCD determination of the CS kernel, which includes systematic control of quark mass, operator renormalization, and discretization effects and uses next-to-next-to-leading logarithmic matching to TMDs from the corresponding lattice-calculable distributions. This allows a parametrization of the CS kernel to be constrained entirely by first-principles calculations for the first time.

The Collins-Soper kernel.—The transverse momentum of a parton of flavor i in a given hadron state is encoded in the TMDs $f_i^{\mathrm{TMD}}(x, b_T, \mu, \zeta)$, which are functions of the longitudinal momentum fraction x carried by the parton, the transverse displacement b_T (the Fourier conjugate of q_T), the virtuality scale μ, and the hadron momentum through the rapidity scale ζ. Unlike the μ evolution of the TMDs, which is perturbative for perturbative scales μ and ζ, the ζ evolution of TMDs is nonperturbative and is encoded in the CS kernel [22,23],

$$\gamma_i(b_T, \mu) = 2 \frac{d}{d \ln \zeta} \ln f_i^{\mathrm{TMD}}(x, b_T, \mu, \zeta). \tag{1}$$

The quark CS kernel $\gamma_q(b_T, \mu)$ is independent of flavor. The kinematic regime of particular interest is for $b_T \gtrsim 0.6$ fm, where there is some tension between different phenomenological parametrizations of the kernel [36–41].

Lattice QCD calculation.—Constraints on the quark CS kernel are extracted from lattice QCD calculations on three ensembles of gauge fields produced by the MILC Collaboration [42] with $2+1+1$ dynamical quark flavors, the one-loop Symanzik improved gauge action [43–46], and the highly improved staggered quark action with sea quark masses tuned to reproduce the physical pion mass [47–49]. The calculations are performed as detailed in Ref. [35], which presented results on one ensemble of lattice gauge fields with four-volume $L^3 \times T = (48a)^3 \times 64a$ with $a = 0.12$ fm. This Letter adds calculations on an additional two ensembles of gauge fields with four-volumes $L^3 \times T = (32a)^3 \times 48a$ with $a = 0.15$ fm and $L^3 \times T = (64a)^3 \times 96a$ with $a = 0.09$ fm, enabling systematic investigation of discretization effects for the first time. A summary of the computation and analysis are included below, with further details and figures provided in Supplemental Material [50], which also includes Refs. [51–62].

Within the large-momentum effective theory [63–65] framework, the lightlike-separated operators that define physical TMDs are related to lattice-calculable "quasi-distributions" defined by matrix elements of purely space-like-separated operators at large hadron momentum $|\mathbf{P}| \gg \Lambda_{\mathrm{QCD}}$ [66–80] with matching coefficients computed perturbatively. Using this approach, the quark CS kernel may be extracted from ratios of matrix elements of staple-shaped Wilson line operators in hadron states at different boost momenta P_1^z, P_2^z [66,68,71],

$$\gamma_q^{\overline{\mathrm{MS}}}(b_T,\mu) = \lim_{a\to 0}\lim_{\ell\to\infty} \frac{1}{\ln(P_1^z/P_2^z)} \ln \frac{\int_{-\infty}^{\infty}\frac{\mathrm{d}b^z}{2\pi}\, e^{i(x-\frac{1}{2})P_1^z b^z} P_1^z N_\Gamma(P_1^z) \sum_{\Gamma'} Z_{\Gamma\Gamma'}^{\overline{\mathrm{MS}}}(\mu,a) W_{\Gamma'}^{(0)}(b_T,b^z,P_1^z,\ell,a)}{\int_{-\infty}^{\infty}\frac{\mathrm{d}b^z}{2\pi}\, e^{i(x-\frac{1}{2})P_2^z b^z} P_2^z N_\Gamma(P_2^z) \sum_{\Gamma'} Z_{\Gamma\Gamma'}^{\overline{\mathrm{MS}}}(\mu,a) W_{\Gamma'}^{(0)}(b_T,b^z,P_2^z,\ell,a)} + \delta\gamma_q^{\overline{\mathrm{MS}}}(\mu,x,P_1^z,P_2^z) + \text{p.c.} \tag{2}$$

Here, the perturbative matching correction is denoted $\delta\gamma_q^{\overline{\mathrm{MS}}}(\mu,x,P_1^z,P_2^z)$, p.c. denotes ($x$-dependent) power corrections proportional to powers of $1/(b_T P^z)^2$ and $(\Lambda/P^z)^2$, where Λ is a generic hadronic scale, $N_\Gamma(P^z)$ are normalization factors corresponding to $N_{\gamma_3\gamma_5}(P^z) = -im_h/P^z$ and $N_{\gamma_4\gamma_5}(P^z) = m_h/E_h(P^z)$, where m_h and $E_h(P^z)$ are the hadron mass and energy, respectively, $Z_{\Gamma\Gamma'}^{\overline{\mathrm{MS}}}(\mu)$ are 16×16 renormalization matrices in Dirac space, and $W_\Gamma^{(0)}(b_T,b^z,P^z,\ell,a)$ denotes ratios of bare quark quasi-TMD wave functions (quasi-TMD WFs),

$$W_\Gamma^{(0)}(b_T,b^z,P^z,\ell,a) = \frac{\tilde{\phi}_\Gamma(b_T,b^z,P^z,\ell,a)}{\tilde{\phi}_{\gamma_4\gamma_5}(b_T,0,0,\ell,a)}. \tag{3}$$

Here $\tilde{\phi}_\Gamma(b_T,b^z,P^z,\ell,a)$ are defined as matrix elements of nonlocal quark bilinear operators $\mathcal{O}_{u\bar{d}}^{\Gamma}(b_T,b^z,\ell)$ with the u and $\bar{d}$ quarks separated by four-vector $b = (\mathbf{b}_T,b^z,0)$ and connected by a staple-shaped Wilson line of total length $\ell + b_T$, between the QCD vacuum and a hadron state at boost P^z,

$$\tilde{\phi}_\Gamma(b_T,b^z,P^z,\ell,a) = \langle 0|\mathcal{O}_{u\bar{d}}^{\Gamma}(b_T,b^z,\ell)|h(P^z)\rangle, \tag{4}$$

computed with lattice discretization scale a. Because the kernel is independent of the choice of hadron state, pion states are used here for simplicity. Similar approaches have been used in previous lattice QCD studies to constrain the quark CS kernel [26–34] and other TMD quantities [28,29,34,81,82].

The numerical calculation proceeds as detailed in Ref. [35]:

Computation of bare quasi-TMD WF ratios.—Bare quasi-TMD WFs $\tilde{\phi}_\Gamma(b_T,b^z,P^z,\ell,a)$ are extracted from bootstrap-level fits to the Euclidean time dependence of two-point correlation functions both with and without staple-shaped operators. Pion states are created with momentum-smeared interpolating fields [83], and the tree-level $\mathcal{O}(a)$-improved Wilson clover fermion action [84–86] is used for propagator computation, with clover term coefficient $c_{sw} = 1.0$. Hopping parameters are $\kappa \in \{0.12575, 0.12547, 0.1252\}$ for calculations on the ensembles with $a \in \{0.15, 0.12, 0.09\}$ fm, respectively, yielding close-to-physical values of the pion mass $m_\pi \in \{172(3), 149(1), 179(1)\}$ MeV, and field configurations are treated with Wilson flow to flow time $\mathfrak{t} = 1.0$ [87] and gauge fixed to Landau gauge before measurements are made. (Gauge fixing is necessary for the computation of the renormalization factors discussed below.)

Calculations are performed on each ensemble for the operator choices (defined by Γ and the staple geometry specified by ℓ, b^z, b_T), choices of momenta P^z, and the numbers of configurations specified in Table I. For the geometries with odd ℓ/a where no $b^z = 0$ matrix elements are available [as used in the denominator of Eq. (3) to form ratios], the average of those with $b^z/a = \pm 1$ are used.

Determination of renormalization factors $Z_{\Gamma\Gamma'}^{\overline{\mathrm{MS}}}(\mu,a)$—. The 16×16 matrices of renormalization factors $Z_{\Gamma\Gamma'}^{\overline{\mathrm{MS}}}(\mu,a)$ are computed using the RI/xMOM renormalization scheme [88–90] and converted to $\overline{\mathrm{MS}}$ using a conversion coefficient computed in continuum perturbation theory [90]. Calculations use $N_{\mathrm{cfg}} \in \{120, 32, 30\}$ gauge field configurations on the ensembles with $a \in \{0.15, 0.12, 0.09\}$ fm, and statistical uncertainties are estimated using bootstrap

TABLE I. Details of the parameters used for calculation on each ensemble of lattice gauge fields. Lattice momenta are specified as n^z, with $P^z = (2\pi/L)n^z$. For operators with staple extent ℓ/a, all geometries with $-\ell/a \le b^z \le \ell/a$ and $0 \le b_T/a \le 7$ along $\hat{n}_T \in \{\pm\hat{x}, \pm\hat{y}\}$ are computed, for all of the 16 Dirac structures Γ. The number of configurations used for each measurement is denoted N_{cfg}; on each configuration, sources on a 2^4 grid bisecting the lattice along each dimension are used.

n^z	P^z (GeV)	ℓ/a	N_{cfg}
$L^3 \times T = (32a)^3 \times 48a,\ a = 0.15$ fm			
0		{7,10,13,14,17,21,25}	229
3	0.77	{21,25}	1105
5	1.29	{14,17}	1105
7	1.81	{10,13}	1105
9	2.32	{7,10}	1105
$L^3 \times T = (48a)^3 \times 64a,\ a = 0.12$ fm			
0	0	{11,14,17,20,26,32}	79
4	0.86	{26,32}	469
6	1.29	{17,20}	472
8	1.72	{14,17}	523
10	2.15	{11,14}	481
$L^3 \times T = (64a)^3 \times 96a,\ a = 0.09$ fm			
0	0	{12,17,22,27,32,35,43}	47
4	0.86	{35,43}	303
6	1.29	{27,32}	472
8	1.72	{17,22}	269
10	2.15	{12,17}	270

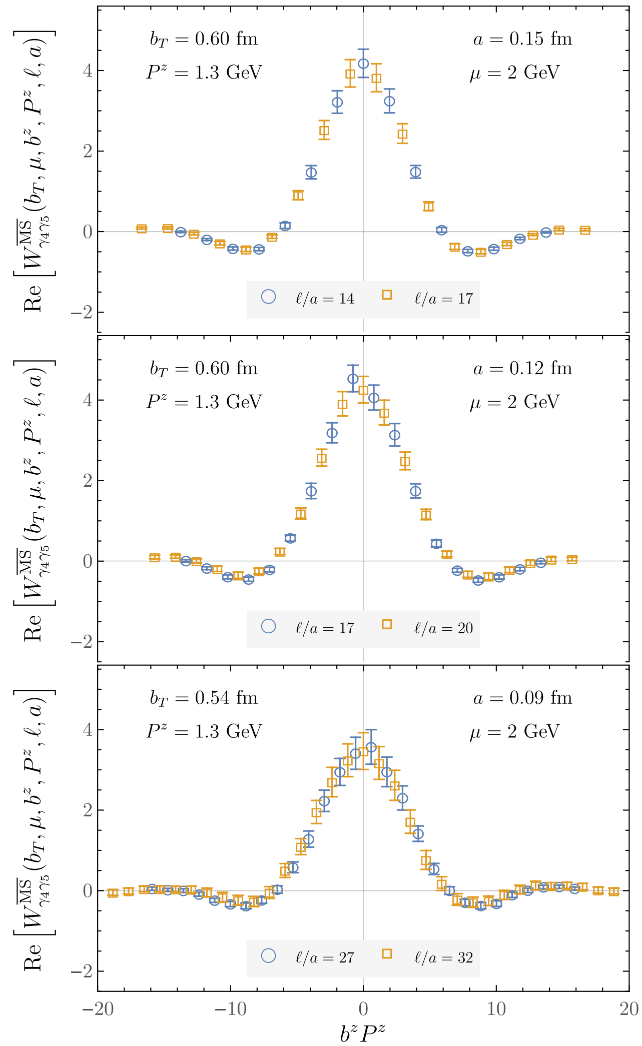

FIG. 1. The real parts of the $\overline{\mathrm{MS}}$-renormalized quasi-TMD WF ratios, $W^{\overline{\mathrm{MS}}}_{\Gamma}(b_T, \mu, b^z, P^z, \ell, a)$, computed on each ensemble. Results on ensembles with $a \in \{0.15, 0.12, 0.09\}$ fm are shown from top to bottom, as functions of b^z, for $\Gamma = \gamma_4\gamma_5$, $P^z = 1.3$ GeV, and similar though not identical b_T values as indicated in each panel.

resampling. Following the procedure detailed in Ref. [35], a range of renormalization scales and off-shell quark momenta are used to compute the renormalization matrices, and a systematic uncertainty, added in quadrature with the statistical uncertainty, is defined as half the difference between the maximum and minimum RI/xMOM renormalization factor over the scales studied. Further details are given in Supplemental Material [50]. Examples of the $\overline{\mathrm{MS}}$-renormalized quasi-TMD WF ratios, $W^{\overline{\mathrm{MS}}}_{\Gamma}(b_T, \mu, b^z, P^z, \ell, a) = \sum_{\Gamma'} Z^{\overline{\mathrm{MS}}}_{\Gamma\Gamma'}(\mu, a) W^{(0)}_{\Gamma'}(b_T, b^z, P^z, \ell, a)$, computed on each ensemble, are shown in Fig. 1.

Fourier transformation.—After renormalization and multiplication by $N_\Gamma(P^z)$, a discrete Fourier transform (DFT) is used to realize the Fourier transforms in the numerator and denominator of Eq. (2), where the quasi-TMD WF ratios for each P^z are first averaged over $\pm b^z$ and the relevant values of $\ell(P^z)$. This yields x-space-renormalized quasi-TMD WF ratios $W^{\overline{\mathrm{MS}}}_{\Gamma}(b_T, \mu, x, P^z, a)$. Because results are computed for a finite range of b^z, the DFT is effectively truncated to a finite range. The effects of this truncation are studied by comparing results using subsets of the data with $b^z < b^z_{\mathrm{max}}$ and varying b^z_{max}, as well as by comparing results where an analytical model is used to extrapolate to $b^z > b^z_{\mathrm{max}}$. Truncation effects are found in this way to lead to negligible systematic uncertainties, as detailed for the $a = 0.12$ fm ensemble in Ref. [35].

Perturbative matching.—The perturbative matching correction $\delta\gamma^{\overline{\mathrm{MS}}}_q(\mu, x, P^z_1, P^z_2)$ appearing in Eq. (2) is taken to be the "b_T-unexpanded resummed next-to-next-to-leading order" (uNNLL) correction detailed in Ref. [35]. It was found in the analysis of Ref. [35], for the same $a = 0.12$ fm ensemble also studied here, that this choice reduces the effect of b_T-dependent power corrections and offers the best convergence compared with other currently available matching prescriptions, i.e., fixed-order [76,91–93] and resummed [61,72,77] corrections up to next-to-next-to-leading order.

Extraction of the CS kernel.—Each choice of x, P^z, and a defines an estimator for the CS kernel [corresponding to the right-hand side of Eq. (2) with the Fourier transform implemented via DFT, neglecting the p.c. term, and without the limit $a \to 0$ being taken],

$$\hat{\gamma}_{\Gamma}^{\overline{\rm MS}}(b_T, \mu, x, P_1^z, P_2^z, a) = \frac{1}{\ln(P_1^z/P_2^z)} \ln\left[\frac{W_{\Gamma}^{\overline{\rm MS}}(b_T, \mu, x, P_1^z, a)}{W_{\Gamma}^{\overline{\rm MS}}(b_T, \mu, x, P_2^z, a)}\right] + \delta\gamma_q^{\overline{\rm MS}}(\mu, x, P_1^z, P_2^z). \tag{5}$$

In principle, it would be desirable to exploit the multiple lattice ensembles available in this calculation to perform a continuum extrapolation of the CS kernel estimator for individual b_T values; this would require matched bT across the ensembles. Alternatively, one might aim to disentangle power corrections and discretization effects by fitting all results for $\mathrm{Re}[\hat{\gamma}_{\Gamma}^{\overline{\rm MS}}(b_T, \mu, x, P_1^z, P_2^z, a)]$ to a parametrization of the CS kernel plus P^z-, a-, and b_T-dependent terms (Specifically, such corrections would be proportional to terms such as a/b_T, a^2/b_T^2, $[1/\ln(P_1^z/P_2^z)]\{[1/b_T^2(P_1^z)^2] - [1/b_T^2(P_2^z)^2]\}$, $[\Lambda^2/\ln(P_1^z/P_2^z)]\{[1/(P_1^z)^2] - [1/(P_2^z)^2]\}$, $[1/\ln(P_1^z/P_2^z)][a(P_1^z - P_2^z)]$, $[1/\ln(P_1^z/P_2^z)][a^2(P_1^z)^2 - a^2(P_2^z)]$, ….). In practice, estimators for different $\{P_1^z, P_2^z\}$ are largely consistent, and as such the data are insufficient to constrain momentum-dependent power corrections.

Instead, the CS kernel on each ensemble is determined as a bootstrap-level weighted average of $\mathrm{Re}[\hat{\gamma}_{\Gamma}^{\overline{\rm MS}}(b_T, \mu, x, P_1^z, P_2^z, a)]$ over $\Gamma \in \{\gamma_4\gamma_5, \gamma_3\gamma_5\}$, all available combinations of $\{P_1^z, P_2^z\}$, and $x \in [0.3, 0.7]$, with weights proportional to the inverse variance, just as done in Ref. [35]. These P_z-, Γ-, and x-averaged CS kernel constraints, denoted $\gamma_q^{\overline{\rm MS}}(b_T, \mu, a)$, should agree with the CS kernel up to discretization effects. The results (including a fit to a parametrization of the CS kernel and the leading a/b_T discretization effects, as discussed in the next section) are shown in Fig. 2.

Additionally, an analogous analysis of $\mathrm{Im}[\hat{\gamma}_{\Gamma}^{\overline{\rm MS}}(b_T, \mu, x, P_1^z, P_2^z, a)]$ can be performed. As the CS kernel is purely real, significant deviation of the resulting numerical results from zero would provide an indication of systematic uncertainties beyond those that are quantified in this calculation. This analysis is presented in Supplemental Material [50]. Including the uNNLL matching of Ref. [35] and recent developments [94] accounting for a linear

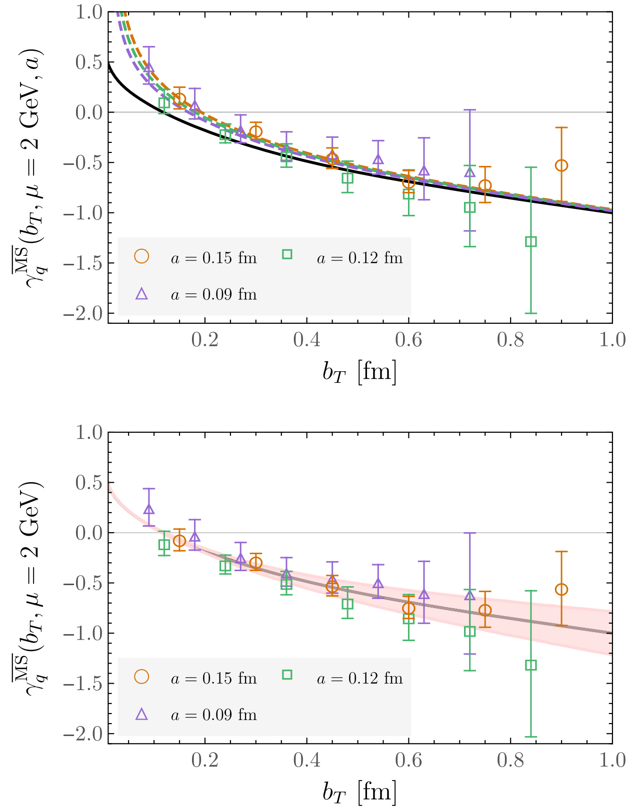

FIG. 2. Upper: averaged CS kernel estimators computed on each ensemble, including a fit to a parametrization of the CS kernel plus $\mathcal{O}(a/b_T)$ discretization effects, as described in the text. The colored dashed curves correspond to $\gamma_q^{\rm param}(b_T, \mu, a)$, with the best-fit values of $(B_{\rm NP}, c_0, c_1, k_1, k_2)$ as described in the text, at each corresponding value of a, while the solid black curve shows the result at $a = 0$. Lower: lattice QCD constraints on the CS kernel, with $\mathcal{O}(a/b_T)$ artifacts subtracted as defined in the text, and the best-fit parametrization of the CS kernel fit to the lattice results shown as a solid black curve, with the 1σ uncertainty band shown as a shaded red region.

infrared renormalon in the imaginary part of the matching coefficient for the quasi-TMD WF, there is no evidence in the numerical data for significant additional unconstrained systematic uncertainties.

Parametrization.—The Lattice QCD constraints on the CS kernel are fit to the parametrization of Ref. [40], with the addition of terms accounting for lattice discretization effects proportional to a/b_T, a^2/b_T^2,

$$\gamma_q^{\rm param}(b_T, \mu, a; B_{\rm NP}, c_0, c_1; k_1, k_2) = -2\mathcal{D}_{\rm res}(b^*, \mu) - 2\mathcal{D}_{\rm NP}(b_T; B_{\rm NP}, c_0, c_1) + k_1 \frac{a}{b_T} + k_2 \frac{a^2}{b_T^2}, \tag{6}$$

where $\mathcal{D}_{\rm res}$ ($\mathcal{D}_{\rm res}$ is given explicitly in Supplemental Material [50]) is the resummed leading power expression for the CS kernel computed in the operator product expansion, evolved to scale μ, and the parametrization of the remaining nonperturbative piece is

$$\mathcal{D}_{\rm NP}(b_T; B_{\rm NP}) = b_T b^* \left[c_0 + c_1 \ln\left(\frac{b^*}{B_{\rm NP}}\right)\right], \tag{7}$$

and

$$b^*(b_T; B_{\mathrm{NP}}) = \frac{b_T}{\sqrt{1 + \frac{b_T^2}{B_{\mathrm{NP}}^2}}}. \tag{8}$$

The expression of Eq. (6) is thus a three-parameter $(B_{\mathrm{NP}}, c_0, c_1)$ parametrization of the CS kernel, with an additional two parameters (k_1, k_2) modeling lattice discretization effects.

The lattice QCD constraints on the CS kernel, for each of the three values of a used in the numerical calculations, are fit simultaneously to Eq. (6) to yield $(B_{\mathrm{NP}}, c_0, c_1, k_1, k_2)$. To diagnose overfitting, additional fits are performed in which subsets of the model parameters are held fixed at reference values, namely, $c_1 = k_1 = k_2 = 0$ and $B_{\mathrm{NP}} = 2$ GeV, while others are optimized. The Akaike information criterion (AIC) [95] is used to quantify the relative goodness of fit for models including different parameter subsets. The minimum AIC model is found to be (c_0, k_1) with $c_1 = k_2 = 0$ and $B_{\mathrm{NP}} = 2$ GeV. The corresponding fit results are

$$c_0 = 0.032(12), \qquad k_1 = 0.22(8), \tag{9}$$

with a $\chi^2/\mathrm{d.o.f.} = 0.39$. These fit results and the resulting parametrization of the CS kernel are shown in Fig. 2, with the 1σ uncertainty band determined as the 68% empirical bootstrap confidence interval from fits performed to $N_{\mathrm{boot}} = 200$ bootstrap samples of the lattice QCD results (constructed to preserve correlations between results at different b_T values computed on the same ensemble). Overall fit quality is illustrated through the comparison of $\gamma_q^{\mathrm{param}}(b_T, \mu, a = 0)$ with best-fit values for $(B_{\mathrm{NP}}, c_0, c_1, k_1, k_2)$ with the lattice QCD results where discretization effects have been subtracted, i.e., $\gamma_q^{\overline{\mathrm{MS}}}(b_T, \mu) \equiv \gamma_q^{\overline{\mathrm{MS}}}(b_T, \mu, a) - k_1(a/b_T)$ using the best-fit results for k_1.

These continuum-limit results are compared with phenomenological parametrizations of experimental data in Fig. 3. In particular, the parametrization used in Ref. [37] corresponds to the AIC-preferred parametrization used here and leads to a consistent result $c_0^{\mathrm{SV19}} = 0.043(11)$ with $B_{\mathrm{NP}}^{\mathrm{SV19}} = 1.9(2)$ GeV. The global fits performed in Ref. [40] also give a consistent result, $c_0^{\mathrm{ART23}} = 0.037(6)$, though in that work c_1 is also included as a fit parameter.

Fits to other parameter subsets (c_0, k_2) and (c_0, k_1, k_2) give consistent results for c_0 at 1σ with uncertainties that differ by $\lesssim 10\%$. The magnitudes of k_1 and k_2 range from 0.1 to 0.3 in all cases, which suggests that the size of discretization effects is consistent with naive dimensional analysis. Fits including B_{NP} or c_1 as free parameters give consistent results for c_0 with larger uncertainties.

Other parametrizations for the nonperturbative function $\mathcal{D}_{\mathrm{NP}}(b)$ have been used in fits to experimental data [36,97], for example the Brock-Nadolsky-Landry-Yuan (BLNY)

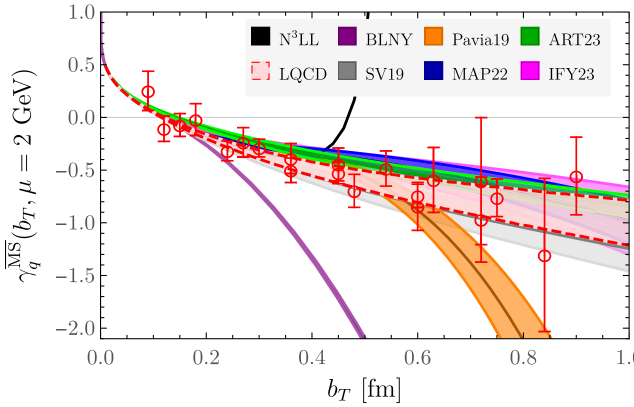

FIG. 3. Comparison of lattice QCD parametrization of the CS kernel compared with phenomenological parametrizations [36–41] of experimental data (BLNY, SV19, Pavia19, MAP22, ART23, IFY23) and perturbative results from Refs. [59,60,96] (N³LL).

parametrization $\mathcal{D}_{\mathrm{NP}}^{\mathrm{BLNY}}(b) = g_2 b^2$ with free parameters g_2 and B_{NP} (which enters $\mathcal{D}_{\mathrm{res}}$). Fits to this parametrization with $B_{\mathrm{NP}} = 1.5$ GeV lead to the result $g_2 = 0.085(26)$ with comparable goodness of fit, $\chi^2/\mathrm{d.o.f.} = 0.58$, to the fits using the parametrization of Eq. (7) described above. This is consistent with the phenomenological fit results of Ref. [41], which use the same value of B_{NP} and find $g_2 = 0.053(24)$. Alternatively, using the parametrization of Ref. [98] yields another consistent result, with $\chi^2/\mathrm{d.o.f.} = 0.38$ [with free parameters as defined in that work such that m_K is held fixed to 0.3 GeV and $b_K = 0.63(19)$ is the result of fitting to the lattice QCD results]. These lattice QCD constraints on the CS kernel are therefore not sufficient to establish a clear preference between functional forms for the kernel; however, they do provide a significant preference for the recent fit results from Refs. [37,39–41] in comparison with Ref. [38] and especially with older BLNY fit results [36] at large b_T.

Summary.—This Letter presents the first lattice QCD calculation of the CS kernel with systematic control of quark mass, operator renormalization, and discretization effects. The results are used to constrain a "pure-theory" parametrization of the CS kernel through a direct fit to lattice QCD results for the first time. These lattice QCD results for the CS kernel are consistent with the most recent phenomenological results. This opens the door for future first-principles QCD predictions of the CS kernel beyond the region constrained by current experiments, as well as joint fits to experimental data and lattice QCD results. As more precise lattice QCD results are achieved at larger values of b_T in future calculations, this promises to be increasingly valuable.

The CHROMA [99], QLua [100], QUDA [101–103], QDP-JIT [104], and QPhiX [105] software libraries were used

in this work. Data analysis used NumPy [106] and JULIA [107,108], and figures were produced using *Mathematica* [109].

We thank Yang Fu for helpful discussions and Johannes Michel, J. Osvaldo Gonzalez-Hernandez, and Ted Rogers for valuable comments on the manuscript. This work is supported in part by the U.S. Department of Energy, Office of Science, Office of Nuclear Physics, under Grants No. DE-SC0011090 and No. DE-AC02-06CH11357 and by Early Career Award No. DE-SC0021006. P. E. S. is supported in part by Simons Foundation Grant No. 994314 (Simons Collaboration on Confinement and QCD Strings). Y. Z. is also supported in part by the 2023 Physical Sciences and Engineering (PSE) Early Investigator Named Award program at Argonne National Laboratory. This document was prepared using the resources of the Fermi National Accelerator Laboratory (Fermilab), a U.S. Department of Energy, Office of Science, Office of High Energy Physics HEP User Facility. Fermilab is managed by Fermi Research Alliance, LLC (FRA), acting under Contract No. DE-AC02-07CH11359. This research used resources of the National Energy Research Scientific Computing Center (NERSC), a U.S. Department of Energy Office of Science User Facility operated under Contract No. DE-AC02-05CH11231, the Extreme Science and Engineering Discovery Environment (XSEDE) Bridges-2 at the Pittsburgh Supercomputing Center (PSC) through allocation TG-PHY200036, which is supported by National Science Foundation Grant No. ACI-1548562, facilities of the USQCD Collaboration, which are funded by the Office of Science of the U.S. Department of Energy. We gratefully acknowledge the computing resources provided on Bebop, a high-performance computing cluster operated by the Laboratory Computing Resource Center at Argonne National Laboratory, and the computing resources at the MIT SuperCloud and Lincoln Laboratory Supercomputing Center [110].

[1] M. Chiosso (COMPASS Collaboration), Phys. Part. Nucl. **44**, 882 (2013).
[2] M. G. Alexeev *et al.* (COMPASS Collaboration), Phys. Lett. B **824**, 136834 (2022).
[3] G. D. Alexeev *et al.* (COMPASS Collaboration), Eur. Phys. J. C **83**, 924 (2023).
[4] G. D. Alexeev *et al.*, Phys. Lett. B **843**, 137950 (2023).
[5] G. D. Alexeev *et al.* (COMPASS Collaboration), Phys. Lett. B **845**, 138155 (2023).
[6] G. D. Alexeev *et al.* (COMPASS Collaboration), arXiv: 2312.17379.
[7] G. D. Alexeev *et al.* (COMPASS Collaboration), arXiv:2401.00309.
[8] E.-C. Aschenauer *et al.*, arXiv:1501.01220.
[9] E.-C. Aschenauer *et al.* (RHIC SPIN Collaboration), arXiv:2302.00605.
[10] J. Dudek *et al.*, Eur. Phys. J. A **48**, 187 (2012).
[11] S. Diehl *et al.* (CLAS Collaboration), Phys. Rev. Lett. **128**, 062005 (2022).
[12] R. Dupré *et al.* (CLAS Collaboration), Phys. Rev. C **104**, 025203 (2021).
[13] P. Chatagnon *et al.* (CLAS Collaboration), Phys. Rev. Lett. **127**, 262501 (2021).
[14] A. Kim *et al.* (CLAS Collaboration), Phys. Lett. B **849**, 138459 (2024).
[15] E. Voutier *et al.* (CLAS, Jefferson Lab Positron Working Group Collaboration), arXiv:2309.14041.
[16] D. Boer, S. J. Brodsky, P. J. Mulders, and C. Pisano, Phys. Rev. Lett. **106**, 132001 (2011).
[17] D. Boer *et al.*, arXiv:1108.1713.
[18] A. Accardi *et al.*, Eur. Phys. J. A **52**, 268 (2016).
[19] L. Zheng, E. C. Aschenauer, J. H. Lee, B.-W. Xiao, and Z.-B. Yin, Phys. Rev. D **98**, 034011 (2018).
[20] R. Abdul Khalek *et al.*, arXiv:2203.13199.
[21] V. D. Burkert *et al.*, Prog. Part. Nucl. Phys. **131**, 104032 (2023).
[22] J. C. Collins and D. E. Soper, Nucl. Phys. **B193**, 381 (1981); **B213**, 545(E) (1983).
[23] J. C. Collins and D. E. Soper, Nucl. Phys. **B197**, 446 (1982).
[24] J. C. Collins, D. E. Soper, and G. F. Sterman, Nucl. Phys. **B250**, 199 (1985).
[25] G. Bozzi and A. Signori, Adv. High Energy Phys. **2019**, 2526897 (2019).
[26] P. Shanahan, M. L. Wagman, and Y. Zhao, Phys. Rev. D **101**, 074505 (2020).
[27] P. Shanahan, M. Wagman, and Y. Zhao, Phys. Rev. D **102**, 014511 (2020).
[28] Q.-A. Zhang *et al.* (Lattice Parton Collaboration), Phys. Rev. Lett. **125**, 192001 (2020).
[29] Y. Li *et al.*, Phys. Rev. Lett. **128**, 062002 (2022).
[30] M. Schlemmer, A. Vladimirov, C. Zimmermann, M. Engelhardt, and A. Schäfer, J. High Energy Phys. 08 (2021) 004.
[31] P. Shanahan, M. Wagman, and Y. Zhao, Phys. Rev. D **104**, 114502 (2021).
[32] M.-H. Chu *et al.* (LPC Collaboration), Phys. Rev. D **106**, 034509 (2022).
[33] H.-T. Shu, M. Schlemmer, T. Sizmann, A. Vladimirov, L. Walter, M. Engelhardt, A. Schäfer, and Y.-B. Yang, Phys. Rev. D **108**, 074519 (2023).
[34] M.-H. Chu *et al.*, J. High Energy Phys. 08 (2023) 172.
[35] A. Avkhadiev, P. Shanahan, M. Wagman, and Y. Zhao, Phys. Rev. D **108**, 114505 (2023).
[36] F. Landry, R. Brock, P. M. Nadolsky, and C. P. Yuan, Phys. Rev. D **67**, 073016 (2003).
[37] I. Scimemi and A. Vladimirov, J. High Energy Phys. 06 (2020) 137.
[38] A. Bacchetta, V. Bertone, C. Bissolotti, G. Bozzi, F. Delcarro, F. Piacenza, and M. Radici, J. High Energy Phys. 07 (2020) 117.
[39] A. Bacchetta, V. Bertone, C. Bissolotti, G. Bozzi, M. Cerutti, F. Piacenza, M. Radici, and A. Signori (MAP Collaboration), J. High Energy Phys. 10 (2022) 127.
[40] V. Moos, I. Scimemi, A. Vladimirov, and P. Zurita, arXiv:2305.07473.

[41] J. Isaacson, Y. Fu, and C. P. Yuan, arXiv:2311.09916.
[42] A. Bazavov et al. (MILC Collaboration), Phys. Rev. D **87**, 054505 (2013).
[43] K. Symanzik, Nucl. Phys. **B226**, 187 (1983).
[44] G. Curci, P. Menotti, and G. Paffuti, Phys. Lett. **130B**, 205 (1983); **135B**, 516(E) (1984).
[45] M. Luscher and P. Weisz, Commun. Math. Phys. **97**, 59 (1985); **98**, 433(E) (1985).
[46] M. Luscher and P. Weisz, Phys. Lett. **158B**, 250 (1985).
[47] E. Follana, Q. Mason, C. Davies, K. Hornbostel, P. Lepage, and H. Trottier (HPQCD Collaboration), Nucl. Phys. B, Proc. Suppl. **129**, 447 (2004).
[48] E. Follana, M. Alford, C. Davies, P. Lepage, Q. Mason, A. Hart, P. Lepage, Q. Mason, and H. Trottier (HPQCD and UKQCD Collaborations), Nucl. Phys. B, Proc. Suppl. **119**, 449 (2003).
[49] E. Follana, Q. Mason, C. Davies, K. Hornbostel, G. P. Lepage, J. Shigemitsu, H. Trottier, and K. Wong (HPQCD and UKQCD Collaboration), Phys. Rev. D **75**, 054502 (2007).
[50] See Supplemental Material at http://link.aps.org/supplemental/10.1103/PhysRevLett.132.231901 for additional results from intermediate stages of analysis, in particular two-point correlation functions and effective energies, bare and renormalized quasi-TMD WF ratios, CS kernel estimators, their imaginary parts, and the perturbative part of the CS kernel.
[51] M. Constantinou, H. Panagopoulos, and G. Spanoudes, Phys. Rev. D **99**, 074508 (2019).
[52] G. P. Korchemsky and A. V. Radyushkin, Nucl. Phys. **B283**, 342 (1987).
[53] S. Moch, J. A. M. Vermaseren, and A. Vogt, Nucl. Phys. **B688**, 101 (2004).
[54] J. M. Henn, G. P. Korchemsky, and B. Mistlberger, J. High Energy Phys. 04 (2020) 018.
[55] A. von Manteuffel, E. Panzer, and R. M. Schabinger, Phys. Rev. Lett. **124**, 162001 (2020).
[56] I. Moult, H. X. Zhu, and Y. J. Zhu, J. High Energy Phys. 08 (2022) 280.
[57] C. Duhr, B. Mistlberger, and G. Vita, Phys. Rev. Lett. **129**, 162001 (2022).
[58] F. Herzog, S. Moch, B. Ruijl, T. Ueda, J. A. M. Vermaseren, and A. Vogt, Phys. Lett. B **790**, 436 (2019).
[59] Y. Li and H. X. Zhu, Phys. Rev. Lett. **118**, 022004 (2017).
[60] A. A. Vladimirov, Phys. Rev. Lett. **118**, 062001 (2017).
[61] I. W. Stewart, F. J. Tackmann, and W. J. Waalewijn, J. High Energy Phys. 09 (2010) 005.
[62] A. H. Hoang, D. W. Kolodrubetz, V. Mateu, and I. W. Stewart, Phys. Rev. D **91**, 094017 (2015).
[63] X. Ji, Phys. Rev. Lett. **110**, 262002 (2013).
[64] X. Ji, Sci. China Phys. Mech. Astron. **57**, 1407 (2014).
[65] X. Ji, Y. S. Liu, Y. S. Liu, J.-H. Zhang, and Y. Zhao, Rev. Mod. Phys. **93**, 035005 (2021).
[66] X. Ji, P. Sun, X. Xiong, and F. Yuan, Phys. Rev. D **91**, 074009 (2015).
[67] X. Ji, L.-C. Jin, F. Yuan, J.-H. Zhang, and Y. Zhao, Phys. Rev. D **99**, 114006 (2019).
[68] M. A. Ebert, I. W. Stewart, and Y. Zhao, Phys. Rev. D **99**, 034505 (2019).
[69] M. A. Ebert, I. W. Stewart, and Y. Zhao, J. High Energy Phys. 09 (2019) 037.
[70] M. A. Ebert, I. W. Stewart, and Y. Zhao, J. High Energy Phys. 03 (2020) 099.
[71] X. Ji, Y. Liu, and Y.-S. Liu, Nucl. Phys. **B955**, 115054 (2020).
[72] X. Ji, Y. Liu, and Y.-S. Liu, Phys. Lett. B **811**, 135946 (2020).
[73] M. A. Ebert, S. T. Schindler, I. W. Stewart, and Y. Zhao, J. High Energy Phys. 09 (2020) 099.
[74] A. A. Vladimirov and A. Schäfer, Phys. Rev. D **101**, 074517 (2020).
[75] X. Ji, Y. Liu, A. Schäfer, and F. Yuan, Phys. Rev. D **103**, 074005 (2021).
[76] X. Ji and Y. Liu, Phys. Rev. D **105**, 076014 (2022).
[77] M. A. Ebert, S. T. Schindler, I. W. Stewart, and Y. Zhao, J. High Energy Phys. 04 (2022) 178.
[78] S. T. Schindler, I. W. Stewart, and Y. Zhao, J. High Energy Phys. 08 (2022) 084.
[79] R. Zhu, Y. Ji, J.-H. Zhang, and S. Zhao, J. High Energy Phys. 02 (2023) 114.
[80] S. Rodini and A. Vladimirov, J. High Energy Phys. 09 (2023) 117.
[81] J.-C. He, M.-H. Chu, J. Hua, X. Ji, A. Schäfer, Y. Su, W. Wang, Y. Yang, J.-H. Zhang, and Q.-A. Zhang (LPC Collaboration), arXiv:2211.02340.
[82] M.-H. Chu et al., arXiv:2302.09961.
[83] G. S. Bali, B. Lang, B. U. Musch, and A. Schäfer, Phys. Rev. D **93**, 094515 (2016).
[84] B. Sheikholeslami and R. Wohlert, Nucl. Phys. **B259**, 572 (1985).
[85] M. Luscher, S. Sint, R. Sommer, P. Weisz, and U. Wolff, Nucl. Phys. **B491**, 323 (1997).
[86] K. Jansen and R. Sommer (ALPHA Collaboration), Nucl. Phys. **B530**, 185 (1998); **B643**, 517(E) (2002).
[87] M. Lüscher, J. High Energy Phys. 08 (2010) 071; 03 (2014) 092(E).
[88] X. Ji, J.-H. Zhang, and Y. Zhao, Phys. Rev. Lett. **120**, 112001 (2018).
[89] J. Green, K. Jansen, and F. Steffens, Phys. Rev. Lett. **121**, 022004 (2018).
[90] J. R. Green, K. Jansen, and F. Steffens, Phys. Rev. D **101**, 074509 (2020).
[91] Z.-F. Deng, W. Wang, and J. Zeng, J. High Energy Phys. 09 (2022) 046.
[92] O. del Río and A. Vladimirov, Phys. Rev. D **108**, 114009 (2023).
[93] X. Ji, Y. Liu, and Y. Su, J. High Energy Phys. 08 (2023) 037.
[94] Y. Liu and Y. Su, J. High Energy Phys. 02 (2024) 204.
[95] H. Akaike, IEEE Trans. Autom. Control **19**, 716 (1974).
[96] J. Collins and T. Rogers, Phys. Rev. D **91**, 074020 (2015).
[97] P. Sun, J. Isaacson, C. P. Yuan, and F. Yuan, Int. J. Mod. Phys. A **33**, 1841006 (2018).
[98] F. Aslan, M. Boglione, J. O. Gonzalez-Hernandez, T. Rainaldi, T. C. Rogers, and A. Simonelli, arXiv:2401.14266.

[99] R. G. Edwards and B. Joo (SciDAC, LHPC, UKQCD Collaborations), Nucl. Phys. B, Proc. Suppl. **140**, 832 (2005).

[100] A. Pochinsky, QLua, https://usqcd.lns.mit.edu/qlua.

[101] M. Clark, R. Babich, K. Barros, R. Brower, and C. Rebbi, Comput. Phys. Commun. **181**, 1517 (2010).

[102] R. Babich, M. Clark, B. Joo, G. Shi, R. Brower, and S. Gottlieb, in *SC11 International Conference for High Performance Computing, Networking, Storage and Analysis* (2011), arXiv:1109.2935.

[103] M. A. Clark, B. Joo, A. Strelchenko, M. Cheng, A. Gambhir, and R. Brower, *Proceedings of the International Conference for High Performance Computing, Networking, Storage and Analysis (SC '16), Article 68* (2016); arXiv:1612.07873.

[104] F. T. Winter, M. A. Clark, R. G. Edwards, and B. Joó, in *2014 IEEE 28th International Parallel and Distributed Processing Symposium* (2014), pp. 1073–1082, 10.1109/IPDPS.2014.112.

[105] B. Joó, D. D. Kalamkar, T. Kurth, K. Vaidyanathan, and A. Walden, in *High Performance Computing*, edited by M. Taufer, B. Mohr, and J. M. Kunkel (Springer International Publishing, Cham, 2016), pp. 415–427.

[106] C. R. Harris *et al.*, Nature (London) **585**, 357 (2020).

[107] J. Bezanson, A. Edelman, S. Karpinski, and V. B. Shah, SIAM Rev. **59**, 65 (2017).

[108] P. K. Mogensen and A. N. Riseth, J. Open Source Software **3**, 615 (2018).

[109] W. R., Inc., *Mathematica*, Version 12.2, Champaign, IL, 2020, https://www.wolfram.com/mathematica.

[110] A. Reuther, J. Kepner, C. Byun, S. Samsi, W. Arcand, D. Bestor, B. Bergeron, V. Gadepally, M. Houle, M. Hubbell, M. Jones, A. Klein, L. Milechin, J. Mullen, A. Prout, A. Rosa, C. Yee, and P. Michaleas, in *2018 IEEE High Performance extreme Computing Conference (HPEC)* (IEEE, Waltham, MA, 2018), pp. 1–6.